Thermal Modeling of Fiber Optic Embedment in Metal Additive Manufacturing

Elias Snider*, Michelle Gegel*, Ryan Holguin †, Cesar Dominguez †, John Bernardin †, Douglas Bristow*, Robert Landers*
*Department of Mechanical Engineering, Missouri University of Science and Technology, Rolla, MO 65409
†Los Alamos National Laboratory, Los Alamos, NM 87545

Abstract

Optical fibers are useful in many sensing applications, including temperature and radiation sensing as well as distributed strain measurements. These optical fibers may be consolidated within an additive manufacturing process to help diagnose and/or monitor the mechanical performance of a part. However, bonding optical fibers to metal parts using laser-based additive manufacturing requires processing temperatures dangerous to the fiber, posing challenges for fiber survival. To protect the fiber and allow bonding with the metal part, the fibers are plated with a nickel coating prior to embedment – a process that is costly to perform. These coatings may also have small internal defects that vary from one fiber to the next. Due to manufacturing cost and lack of repeatability, it is difficult to experimentally determine appropriate process parameters, such as laser power and coating thickness. Thus, numerical modeling offers an efficient approach to exploring embedment parameters and their effect on fiber survivability. This work employs transient thermal models of embedment processes to identify and simulate significant design parameters such as coating thickness, embedment geometry, and cooling time. A transient thermal simulation was developed and is presented which models fiber optic embedment processes via Laser Engineered Net Shaping (LENS®, a blown powder, direct energy deposition process) and trends in peak fiber core temperatures, as well as thermal shock are discussed.

Introduction

Optical fiber cable is useful in strain, temperature, and radiation sensing applications. Embedded optical fibers have a few distinct advantages over resistive strain elements in high-value and specialty situations: optical fibers are capable of distributed strain sensing using Bragg gratings or Rayleigh Backscattering, can be used in relatively high temperatures, and are impervious to electromagnetic interference. These characteristics are desirable for some high-value, additively manufactured parts, especially where the distributed strain sensing capabilities of these fibers can be used to reveal the presence and location of local strain concentrations via distributive strain mapping.

The silica core within an optical fiber is quite fragile and –without protection –is prone to breakages. Typically, optical fibers are protected by a thin polymer coating which serves to protect the fiber core from damage for most general-use purposes. When using fibers for strain sensing in additively manufactured parts, this polymer coating is often insufficient to protect the fiber degradation or complete loss of signal due from thermal stresses. Ultrasonic additive manufacturing processes have been shown to be capable of embedding uncoated optical fibers within aluminum parts, but metal coatings are necessary for laser melting additive manufacturing environments [1-2]. Nickel plating is a good solution to this problem, offering significant

protection to the silica fiber while also providing a coating which is readily bonded atomically to other metals. Copper plated fibers are commercially available and can be plated with nickel up to substantial diameters well suited for embedment in metal parts. Fiber Bragg Gratings have been used in additively manufactured stainless steel parts to yield strain and temperature measurements as well as to decouple strain and temperatures in the work of Havermann et. al. [3]. Havermann's work also indicated a 350 μm diameter threshold in the nickel coatings which allowed for survival of the fiber during a powder bed fusion process (in which powder is deposited over the entire build surface before melting selected areas with and overhead laser) [3].

Similar fibers have been embedded experimentally by Elias Snider and Michelle Wainwright, although using a direct energy deposition process (use of a blown powder process to additively manufacture parts) on a LENS© machine rather than powder bed fusion. In performing this experimental work, the value of a numerical model was recognized as a way to efficiently explore full ranges and combinations of process parameters, while eliminating the lack of repeatability inherent to the experiments. Thus the geometry, material properties and build parameters selected for the model are based on the set-up used to embed fibers in experimental work. This was achieved via a transient thermal model in Abaqus, a numerical modeling software. Key fiber parameters explored were the fiber coating diameter and the fit of the groove in which the fiber was placed prior to consolidation. The resulting temperatures and thermal shock were examined because these properties are correlated to survivability and transmission degradation of the fiber.

Model Assumptions and Setup

The approach taken in practice while embedding these fibers is to first build a base and groove structure for the fiber to rest within. The build is paused following the completion of the groove structure, the fiber is positioned within the groove as shown in Figure 1, and the build is then resumed to consolidate the fiber within the stainless-steel structure. For this specific application, the additively manufactured part was to be an ASTM E8/E8M-16a tensile specimen, which (at the neck section) has a thickness of 10mm (Figure 1). A portion of this neck section was modeled with a 10 mm-wide block with a fiber placed within the material (Figure 2).

Figure 1: Tensile Specimen and Coated Optical Fiber Before and After Embedment

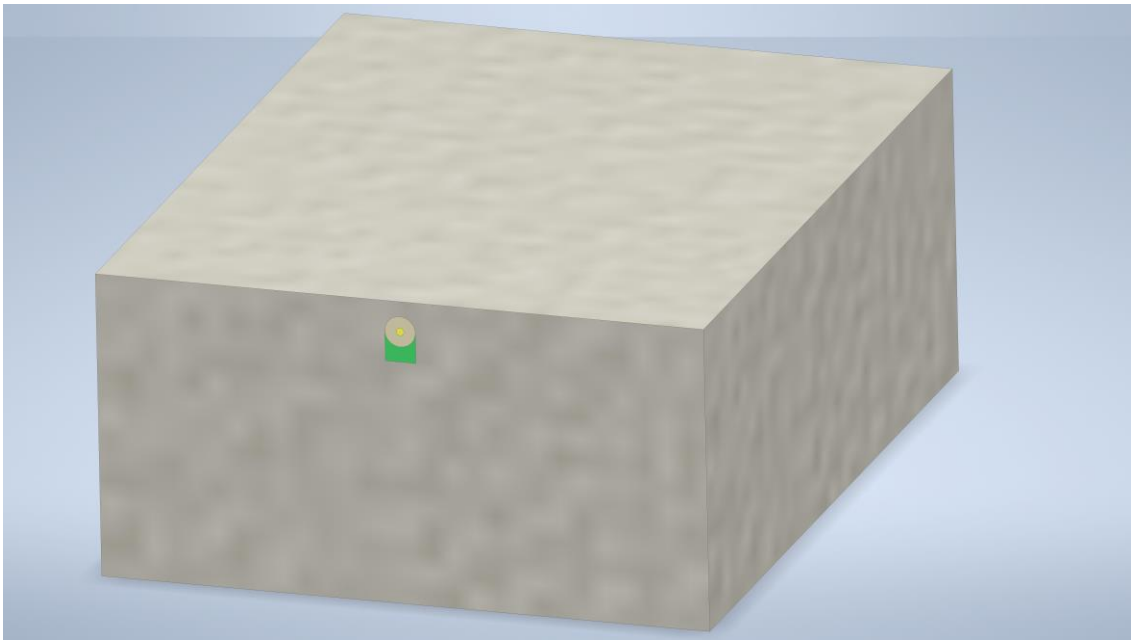

Figure 2: Embedded Optical Fiber CAD Model

The powder used is 316L SS with a particle size of 50-150μm. The fiber has a cladding/core diameter of 125 μm a very thin copper coating (15-50 μm) which was neglected in the modeling analysis, and nickel coating of thickness varying from 300 to 900 μm in outer diameter. The laser power used is 300 W and is a continuous, rather than pulsed, output. The raster paths are perpendicular to the fiber.

This model assumes that the material has already been deposited, is non-porous, and will then be heated by a laser. Figure 3 shows the simplified embedment used in this thermal model. All materials are assumed to be completely rigid and stationary with respect to each other and powder mechanics were neglected. Thermal resistances at material interfaces were neglected. The gap underneath the fiber was assumed to be purely conductive, i.e., radiation and convection were ignored.

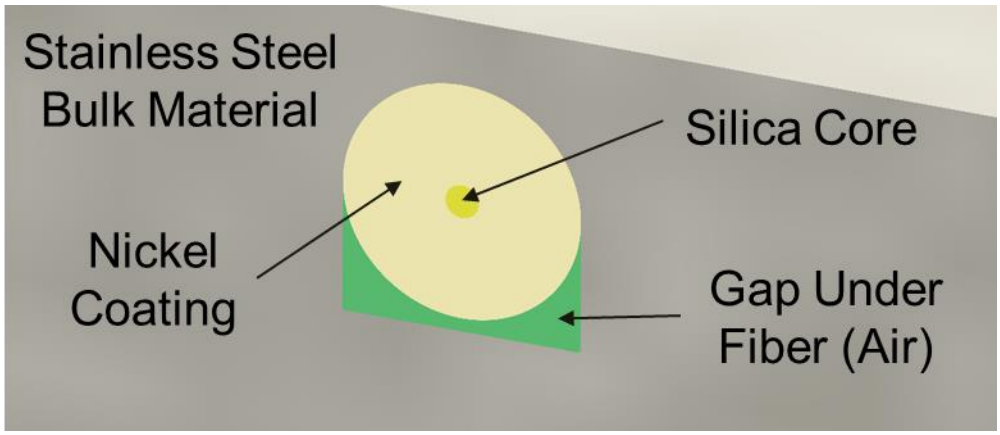

Figure 3: Cross-Section of Embedded Fiber Model

Using Abaqus subroutines, a 300 W laser was simulated to run from the left to the right in Figure 4. A “top-hat”, or uniform power distribution was used, and the laser was assumed to be non-pulsing. The laser source was set up as a surface flux rather than a body flux. The metal reflectivity was then calibrated against an actual melt pool by using optical data from an inline camera on the LENS© machine to match dimensions of the melted regions. Optical fiber dimensions were taken from the datasheets of the fibers used in experimentation and material properties were assumed to be standard values for listed materials. For boundary conditions, the sides and base were considered adiabatic while the top surface was subjected to light convection (20 $W/m^2 K$) and the laser surface flux. In addition, the model was assumed to be symmetric about the front face (a half-model approach).

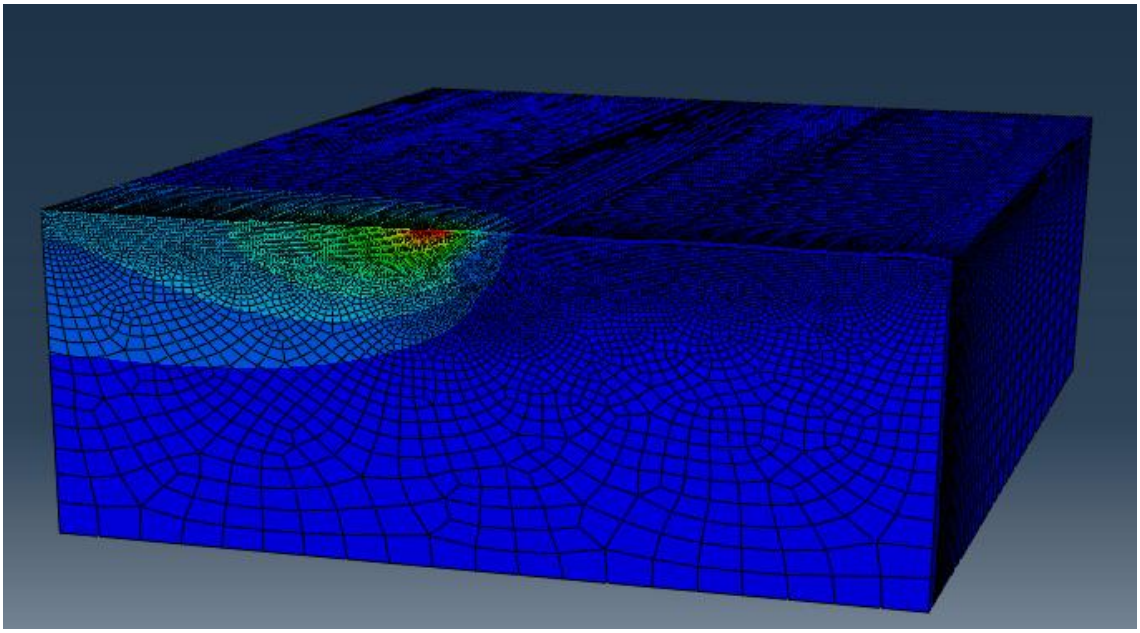

Figure 4: Laser Pass Over Embedded Fiber

Two parameters were of interest in this study of the embedment process: nickel coating diameter and groove fit underneath the optical fiber. In the coating diameter considerations, the groove depth underneath the fiber was kept constant at 500 µm as well as the silica fiber core diameter (125 µm). The outer diameter of the nickel coating was then varied from 150 µm to 900 µm; the groove width was varied with the coating diameter such that the sides of the groove were tangent to the nickel coating in every coating thickness trial to represent more closely what is done in practice with these embedment trials (Figure 5).

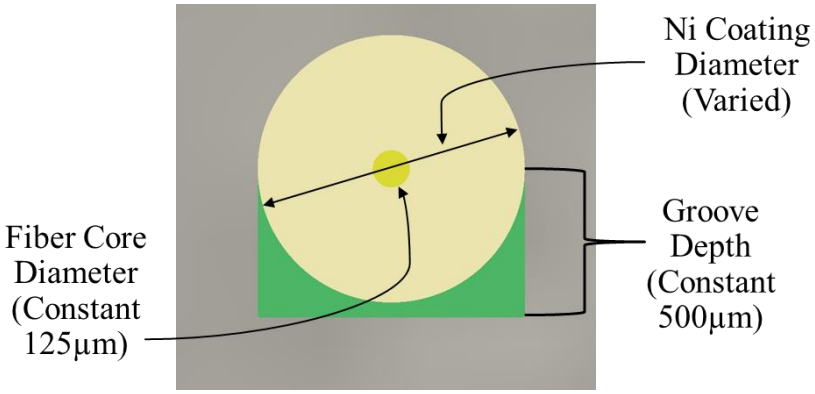

Figure 5: Embedded Fiber Parameters for Coating Thickness Trials

In the second set of simulations, the groove fit was varied to determine if any correlation exists between the fit of the groove and the peak temperatures of the fiber core. In these trials, the fiber core diameter was kept constant at 125 µm and nickel coating diameters were kept constant at 250 and 500 µm (to determine if the effects were similar in differing coating thicknesses). The groove fit was varied from 250 µm down to 50 µm in depth (Figure 6); these results were also compared to the 250 and 500 µm square-bottomed grooves in the first set of simulation results (Figure 5).

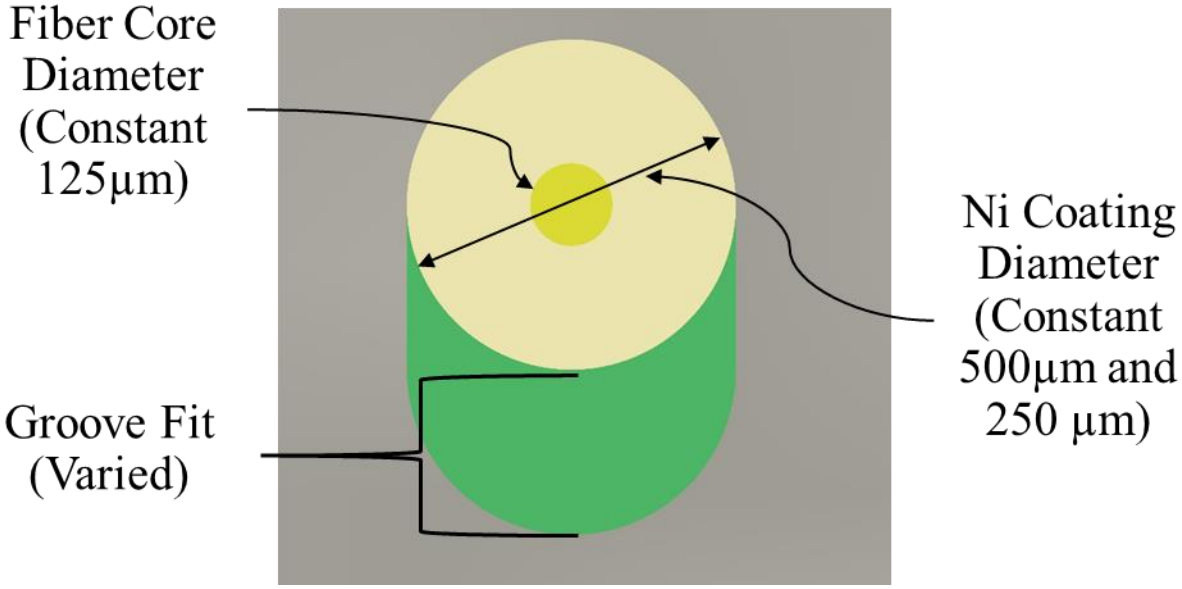

Figure 6: Embedded Fiber Parameters for Groove Fit Trials

Results

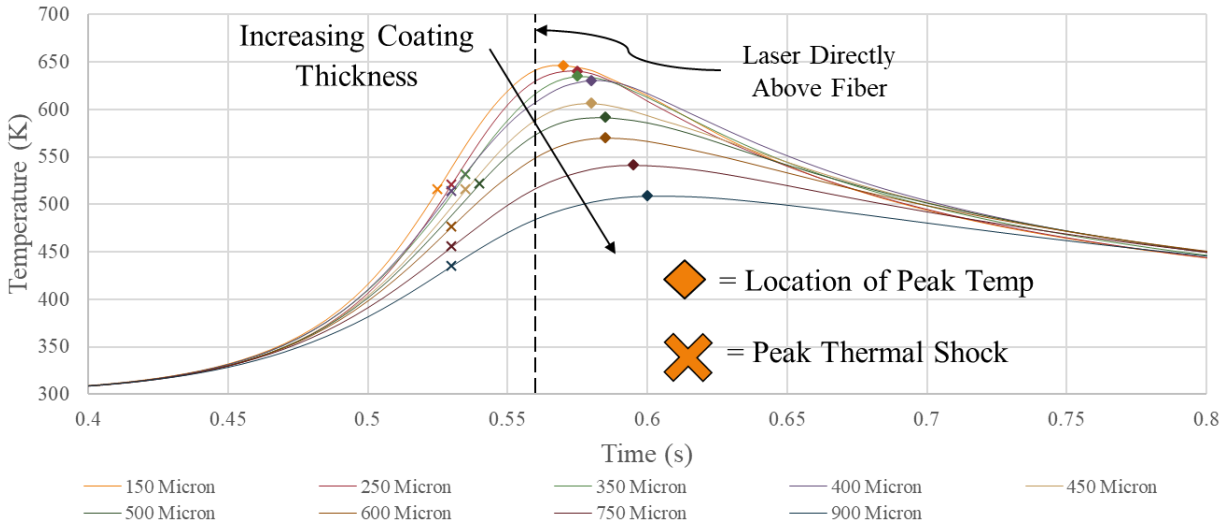

Figure 7: Peak Fiber Temperatures over a Laser Scan

The peak temperatures in the fiber core at any location were plotted against time (Figure 7). These curves revealed a peak core temperature which occurs significantly after the point at which the laser is directly above the fiber (denoted by diamond-shape markers). The time derivative of these curves yields the thermal shock experienced by the fiber core. The location of the maximum thermal shock is indicated by "x"-shaped markers and occurs significantly before the point at which the laser is directly above the fiber.

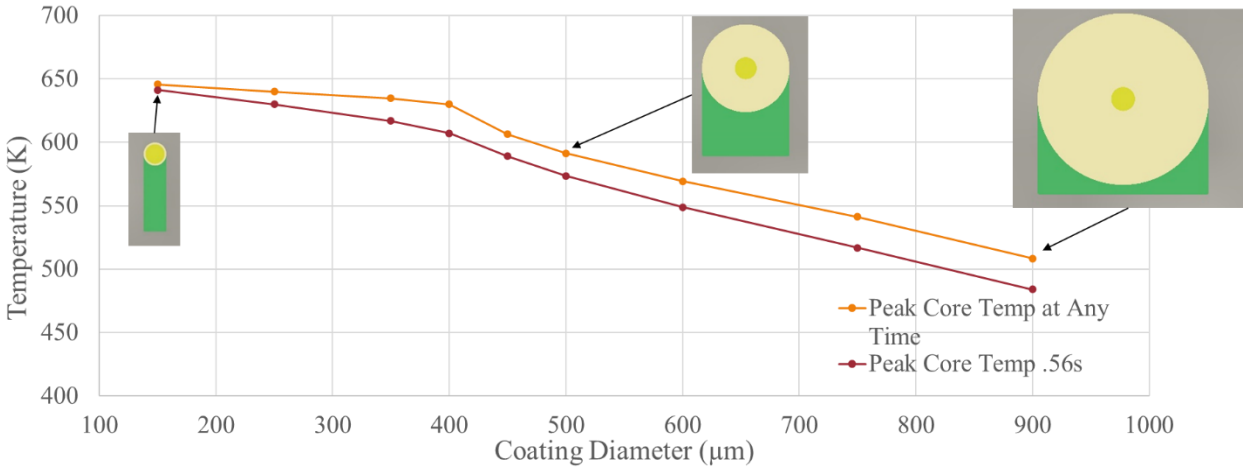

Peak Temperatures for Varied Coating Thicknesses

It can be seen from Figure 8 that there are only marginal returns for increased nickel fiber coating until the diameter of the coating reaches 400 µm. After this point, the peak temperature of the fiber is reduced more sharply with increased coating diameter. The sensitivity to increased nickel coating diameter is approximately $-0.211°C/\mu m$. The peak temperature at any point in time decreases approximately 20% over the range of diameters considered. The difference in temperature between the point in time at which the laser is directly over the fiber and the peak

temperature at any point in time also generally increases over the range and is a result of a decreased thermal shock (decrease in the time derivative of the peak temperature).

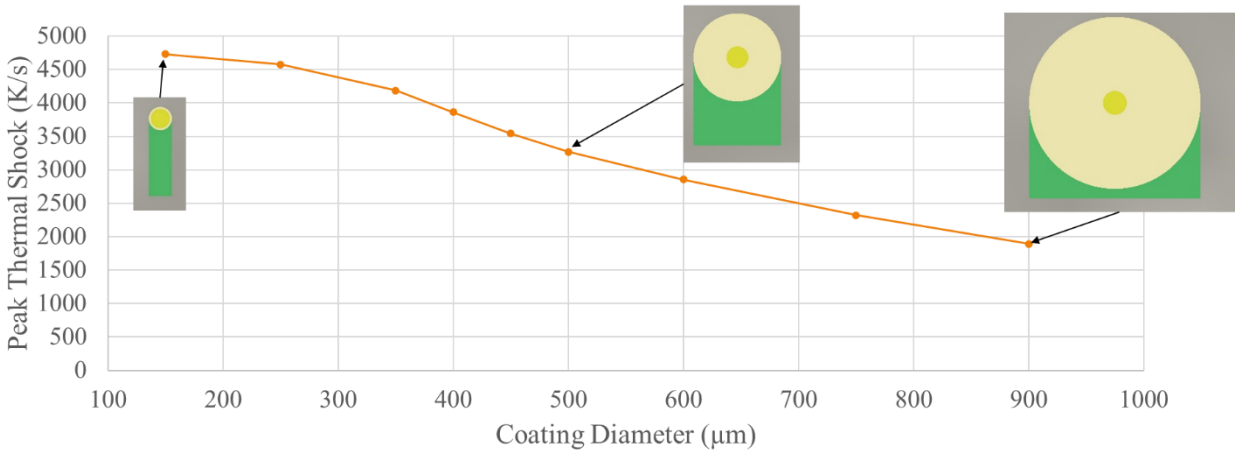

Figure 9: Peak Thermal Shock for Varied Coating Diameter

Figure 9 shows the thermal shock associated with the peak temperature at any point in time in the fiber core for varied coating diameters. The peak thermal shock in the fiber core had a more linear trend than the peak temperature data, with steady reductions for increases in coating diameter. The sensitivity here to increased nickel coating thickness is approximately 4.1 (K/s)/µm. Most notably, the thermal shock was much more sensitive to the coating diameter than peak fiber core temperatures, falling approximately 60% over the same range of fiber diameters.

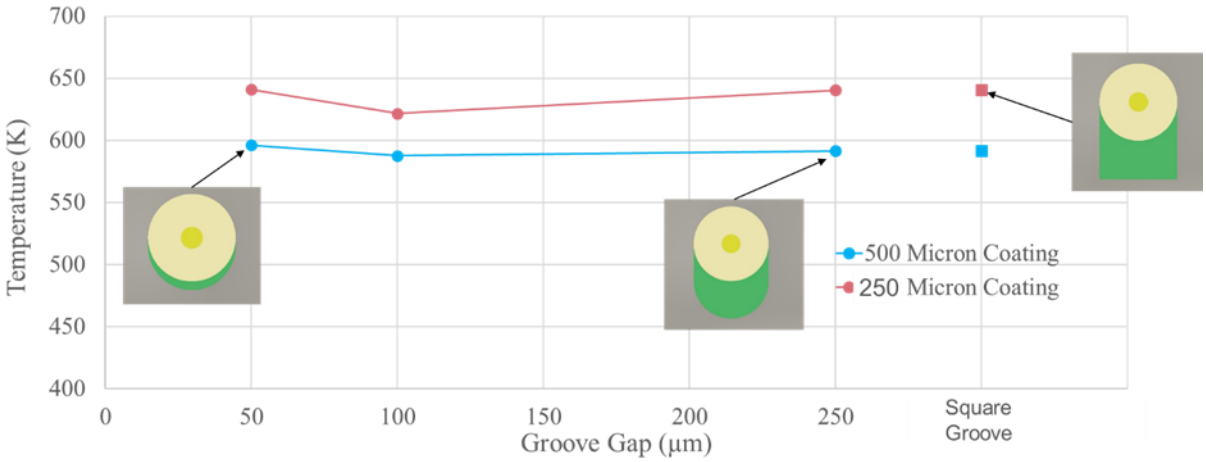

Figure 10: Temperature Profiles for Varied Groove Gaps

There is very little correlation between groove fit and peak temperatures in the fiber. This model does ignore mechanical aspects of fiber embedment, however, and as a result, there may be mechanical factors introduced with poor groove fits which result in fiber core fractures. It should be noted that this model assumed that all bodies were completely rigid and adhered with respect to one another and consequently, residual stresses and shear stresses may be present in the fiber core which would not have manifested as critical points in this thermal model. In both fiber coating diameters considered, though, the groove fit had little impact on the peak temperature of the fiber core.

Conclusions

Direct energy deposition of optical fibers has been achieved through the embedment processes modeled here. Because of the large amounts of time and cost associated with performing experiments, the embedment parameters were instead modeled using a transient thermal model with simplified property assumptions. These models yielded temperature estimates which were then used to uncover general trends in the fiber peak temperatures and thermal shock values. The general trends obtained from these simulations serve to narrow parameter selections and better understand sources of fiber failure while embedding single-mode fibers with additive manufacturing processes.

Increased nickel coating diameters reduced peak temperatures in the fiber and had the greatest effect on peak temperatures after 400 μm. The peak temperature was also reduced as much as 21% over the range of fiber coating diameters considered. In areas where a slow degradation of the optical transmission is observed, much larger diameters could be selected to assist in mitigating these effects.

Increased nickel coating diameters had a more dramatic effect on thermal shock, reducing the shock relatively steadily as the nickel coating diameter increased. The peak thermal shock was reduced by 60% over the range of fiber coating diameters considered and was more sensitive to coating diameter than peak temperature. In areas where a sharp, complete attenuation of the optical transmission is observed, a slightly larger nickel coating diameter could be selected to help preserve the fiber transmission after embedment.

With regards to thermal considerations, the shape and fit of the groove did not affect the fiber temperatures; therefore, when considering embedment parameters pertaining to thermal effects, the shape and fit of the fiber groove may be neglected from considerations.

References

[1] X. L. He et al, "Optical Fiber Sensor for Strain Monitoring of Metallic Device Produced by Very High-Power Ultrasonic Additive Manufacturing," IEEE Sensors Journal, vol. 19, (22), pp. 10680-10685, 2019.

[2] R. Zou et al, "A Digital Twin Approach to Study Additive Manufacturing Processing Using Embedded Optical Fiber Sensors and Numerical Modeling," Journal of Lightwave Technology, vol. 38, (22), pp. 6402-6411, 2020.

[3] D. Havermann et al, "Temperature and Strain Measurements With Fiber Bragg Gratings Embedded in Stainless Steel 316," Journal of Lightwave Technology, vol. 33, (12), pp. 2474-2479, 2015.